

similar structure is observed at both occultation points [see model constants in (35)]. With regard to the region between 20 and 60 km, the deviations from the model curves are similar at both occultation points. Astute readers can infer the type of thermal structure required to explain these deviations by comparison with the reference model curves shown.

37. G. N. Brown and W. T. Ziegler [in *Advances in Cryogenic Engineering*, Vol. 25, K. D. Timmerhaus and H. A. Snyder, Eds. (Plenum, New York, 1979), p. 662] give polynomial fits to vapor pressure data.
38. G. F. Lindal *et al.*, *J. Geophys. Res.* **84**, 9443 (1979).
39. V. R. Eshleman, *Icarus* **80**, 439 (1989).
40. W. B. Hubbard *et al.*, *ibid.*, in press.
41. W. R. Thompson *et al.*, *Geophys. Res. Lett.* **16**, 981 (1989).
42. This experiment required extensive support from NASA headquarters and, at the Jet Propulsion Laboratory (JPL), from the Voyager Project, the Office of Tracking and Data Acquisition, and the Deep Space Network. Members of the Radio Science

Support Team at JPL charged with the implementation and execution of the experiment included A. Densmore, M. Delitsky, P. Eshe, and Y. H. Son, and we thank them and their colleagues for major, sustained efforts in carrying out this experiment; two other members of this team, S. Asmar and D. Morabito, deserve special credit for their critical roles in the encounter preparation and real-time operations. Voyager Project Management contributed to a highly enhanced scientific return by agreeing to and supporting an extremely challenging encounter scenario. The personnel of the Deep Space Communication Complex at Tidbinbilla and at the CSIRO Parkes Radio Astronomy Observatory (RAO) in Australia deserve special mention; their participation and efforts to improve radiometric performance far exceeded the demands of their normal duties. For the first time, we were joined by colleagues from the Japanese Institute of Space and Astronautical Science, who provided the facilities of the Usuda Deep Space Station and who were responsible for the development and execution of the observations in Japan. We are pleased with the

technical exchange and relationships this collaboration brought about. The Radio Science experiments could not have succeeded without the ability to use navigation data taken within about 30 hours of closest approach to fine-tune the spacecraft events for the exacting geometry of a flyby only 4900 km above the cloud tops of Neptune. A 16-s error in estimated arrival time would have resulted in a complete loss of the primary occultation data (and the error was this large 2 days before closest approach); as it developed, the actual arrival time was within 1 s of the last arrival time prediction. The Voyager Navigation Team accomplished this extraordinary feat. F. Donovan, of the S. S. Freedom Office, NASA, performed a real-time liaison function between JPL and Parkes RAO. At Stanford, M. Maurer and T. Spilker contributed importantly to pre-encounter analyses and preparation, encounter operations, and data reduction; H. Rand provided much support, coordination, and help in the preparation of the experiment and of this manuscript.

31 October 1989; accepted 15 November 1989

Magnetic Fields at Neptune

NORMAN F. NESS, MARIO H. ACUÑA, LEONARD F. BURLAGA,
JOHN E. P. CONNERNEY, RONALD P. LEPPING, FRITZ M. NEUBAUER

The National Aeronautics and Space Administration Goddard Space Flight Center—University of Delaware Bartol Research Institute magnetic field experiment on the Voyager 2 spacecraft discovered a strong and complex intrinsic magnetic field of Neptune and an associated magnetosphere and magnetic tail. The detached bow shock wave in the supersonic solar wind flow was detected upstream at 34.9 Neptune radii (R_N), and the magnetopause boundary was tentatively identified at 26.5 R_N near the planet-sun line (1 $R_N = 24,765$ kilometers). A maximum magnetic field of nearly 10,000 nanoteslas (1 nanotesla = 10^{-5} gauss) was observed near closest approach, at a distance of 1.18 R_N . The planetary magnetic field between 4 and 15 R_N can be well represented by an offset tilted magnetic dipole (OTD), displaced from the center of Neptune by the surprisingly large amount of 0.55 R_N and inclined by 47° with respect to the rotation axis. The OTD dipole moment is 0.133 gauss- R_N^3 . Within 4 R_N , the magnetic field representation must include localized sources or higher order magnetic multipoles, or both, which are not yet well determined. The obliquity of Neptune and the phase of its rotation at encounter combined serendipitously so that the spacecraft entered the magnetosphere at a time when the polar cusp region was directed almost precisely sunward. As the spacecraft exited the magnetosphere, the magnetic tail appeared to be monopolar, and no crossings of an imbedded magnetic field reversal or plasma neutral sheet were observed. The auroral zones are most likely located far from the rotation poles and may have a complicated geometry. The rings and all the known moons of Neptune are imbedded deep inside the magnetosphere, except for Nereid, which is outside when sunward of the planet. The radiation belts will have a complex structure owing to the absorption of energetic particles by the moons and rings of Neptune and losses associated with the significant changes in the diurnally varying magnetosphere configuration. In an astrophysical context, the magnetic field of Neptune, like that of Uranus, may be described as that of an “oblique” rotator.

NEPTUNE HAS BEEN DISCOVERED to have an intrinsic planetary magnetic field B and magnetosphere on the basis of data obtained during the close approach by Voyager 2 (V2) on 25 August 1989. The instrumentation (1) for magnetic field measurements on Neptune, which had been used to make observations of the magnetic fields of Jupiter (2), Saturn (3), and Uranus (4), operated normally

throughout the entire encounter. The dual low-field magnetometers (LFMs) may automatically change ranges every 4.8 s, as required by the magnitudes of the measured magnetic field components. The minimum quantization uncertainty is ± 0.002 nT in the lowest range (± 8 nT full scale) and increases to ± 12.2 nT in the highest range of $\pm 50,000$ nT, used near closest approach (CA). The twin high-field magnetometers

(HFMs) also provided data during this encounter (the large fields measured near CA were well within their lower range of $\pm 50,000$ nT, with a quantization uncertainty of ± 12.2 nT). Vector measurements for the LFMs were obtained at intervals of 60 ms and were subsequently averaged over 1.92 s, 9.6 s, 48 s, 8 min, and 1 hour for this study. The HFM measurements were made at 0.6-s intervals and are primarily used within 2 R_N of the planet, where the field is larger than 2000 nT.

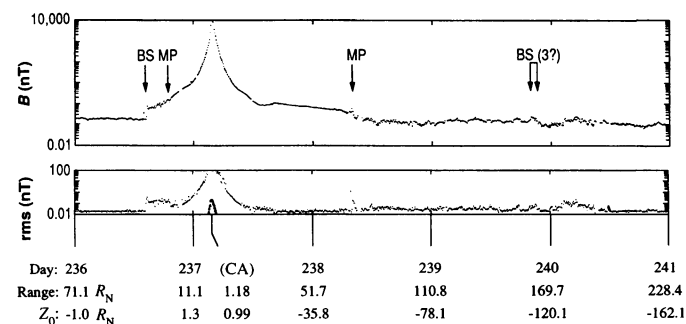
The spacecraft trajectory during flyby and the obliquity of Neptune led to a sequence of observing positions within the magnetosphere that ranged from 26°S while inbound, increasing up to a maximum northerly latitude of 79°N near CA, and then decreasing to 21°S outbound. The spacecraft was within the magnetosphere and magnetotail of the planet for approximately 38 hours. There were no close encounters with any Neptunian moon, as by Voyager 1 at Titan (5), although the trajectory had been chosen so that it passed to within 38,000 km of Triton. Before the V2 encounter, very little was known about the possible existence and characteristics of any Neptunian magnetic field and radiation belts because indisputable identification of nonthermal radio emissions was lacking (6). A number of predictions of the magnetic field at Neptune had been made before encounter (7), covering a range of values from 0.3 to 17 G.

This preliminary report is based on data

N. F. Ness, Bartol Research Institute, University of Delaware, Newark, DE 19716.
M. H. Acuña, L. F. Burlaga, J. E. P. Connerney, R. P. Lepping, Laboratory for Extraterrestrial Physics, NASA Goddard Space Flight Center, Greenbelt, MD 20771.
F. M. Neubauer, Institut für Geophysik und Meteorologie, Universität zu Köln, D-5000 Köln 41, Federal Republic of Germany.

known originally to contain spurious noise, although every reasonable attempt has been made to identify and delete obviously bad data before analysis. Equally important for the quantitative analysis of the planetary field is the preliminary nature of the spacecraft position and attitude information, especially during the several roll and many image-motion-compensation maneuvers that the spacecraft performed during flyby. Thus we are unable, at this time, to provide a complete model of the Neptunian field that is valid near the planet. An offset tilted dipole (OTD) model is valid between 4 and 15 R_N . The observed field departs progressively from this OTD both inside and outside of this range. Derivation and use of the L parameter (the distance in R_N where a given field line crosses the magnetic equator) based on the OTD for interpretation of observations of energetic particles near CA is therefore inappropriate and most likely incorrect. Indeed, even at 4 to 8 R_N the computed L values may be misleading, depending on the equatorial pitch angle (or mirror value of B) of the particles studied.

Magnetopause and bow shock. Figure 1 shows the magnitude of the magnetic field and the associated Pythagorean root-mean-square (rms) deviation, based on 8-min averages, for 5 days around CA. The maximum field magnitude observed, based on these 8-min averages, was 9700 nT. The disturbed nature of the field seen after the last outbound bow shock (BS) (at 2100 UT on day 239 = 239/2100) and ending near 240/1200 is possibly due to waves in the solar wind associated with field line connection to the BS and traditionally referred to as upstream waves. (All times are spacecraft event times in universal time.) Figure 2 shows the modeled magnetopause (MP) and BS boundaries, the trajectory of the spacecraft, and the hourly averaged magnetic field values, in a coordinate system whose symmetry axis, the X_0 axis, is the planet-sun line (the X_0 - ρ plane rotates so as to always contain the sun, Neptune, and the V2). The field magnitude is scaled logarithmically.



in the field, during the relatively long averaging interval used. These values are shown "folded over" in the center of the panel.

Table 1. Neptune magnetosphere boundaries.

Nature of "boundary"	Time (day/hour)	R (R_N)	Spacecraft position, Neptune-centered (R_N)			ρ (R_N)
			X_0	Y_0	Z_0	
BS	236/1438	34.9	33.9	8.3	0.37	8.3
MP	236/1800 -1935*	26.5 \leftrightarrow 23.0	25.7	6.1	0.69 \ddagger	6.1
(CA)	237/0355	1.18	-0.34	-0.55	0.99	1.13
MP	238/0819	72.3	-50.5	10.8	-50.5	51.6
BS (3?)	239/~2000 -2100 \dagger	161.1	-111.0	25.2	-114.0 \S	116.3

*Range of times given because of the complex nature of the inbound boundary, still under study. \dagger Range of times given because of multiple crossings. \ddagger Position of spacecraft given for the earliest time in range. \S Position of spacecraft given for center time in range.

Table 1 gives the center times (or ranges) of the boundaries along the trajectory and V2's position in terms of Neptune's orbital plane X_0 - Y_0 coordinates ($Z_0 = X_0 \times Y_0$), R (V2 distance in units of planetary radius, R_N), and ρ [$= (Y_0^2 + Z_0^2)^{1/2}$]. Ranges are given for MP and BS because of some uncertainty in identification or because of multiple crossings.

One of the most unexpected results from this investigation was that the planet's magnetic dipole axis is tilted far (47°) from the rotation axis (see below). Hence, the magnetosphere, which acts as an obstacle deflecting the solar wind flow, presents radically different aspects or angles of attack to the solar wind as the planet and its magnetic field rotate. The location and shape of the MP vary with time even for a constant solar wind pressure, and the BS varies in response to the motion of the MP.

The BS and MP boundaries are modeled in Fig. 2 as rotationally symmetric ellipsoids (about the X_0 axis) constrained to pass through the identified boundaries. The slope of the ellipsoid at the outbound MP crossing was constrained to be consistent with the estimated normal to that boundary. This was determined from a variance analysis of the 1.92-s averaged field data. The ρ - X_0 component of the normal is shown at the outbound MP as an arrow in Fig. 2; the components of this unit normal are (0.22,

-0.29, 0.93). Aberration of the boundaries due to planetary motion is very small ($\approx 0.7^\circ$) and has been ignored in the modeling. The subsolar BS and MP distances derived from the models were 34.2 and 26.0 R_N , respectively.

Care was taken to properly choose the appropriate boundary "crossing times" for the purpose of modeling. For the outbound BS, the center time of a closely spaced set of crossings was chosen. For the inbound MP position, we assume that the outermost part of the range given in Table 1 is most likely to represent the effective obstacle boundary position.

The magnetic field inside the MP in the broad boundary region from $\sim 236/1800$ to

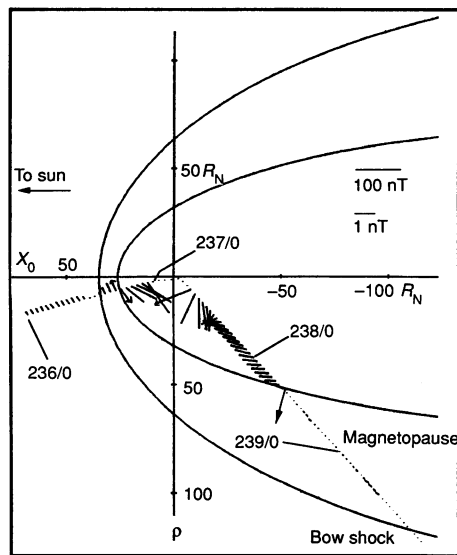


Fig. 2. The trajectory of V2 through the Neptunian magnetosphere and representations of the planetary bow shock, magnetopause, and hourly averaged and logarithmically scaled magnetic field (open-headed arrows shown for some). The plane of projection, for the trajectory and the field, contains the sun, Neptune, and the spacecraft. The magnetopause and bow shock boundaries are represented by portions of ellipses (see text) that are analytically "similar" to each other. The outbound magnetopause normal is indicated by an arrow.

~236/1930 resembles that in the “entry layer” of Earth’s distant polar cusp (8) in the following respects:

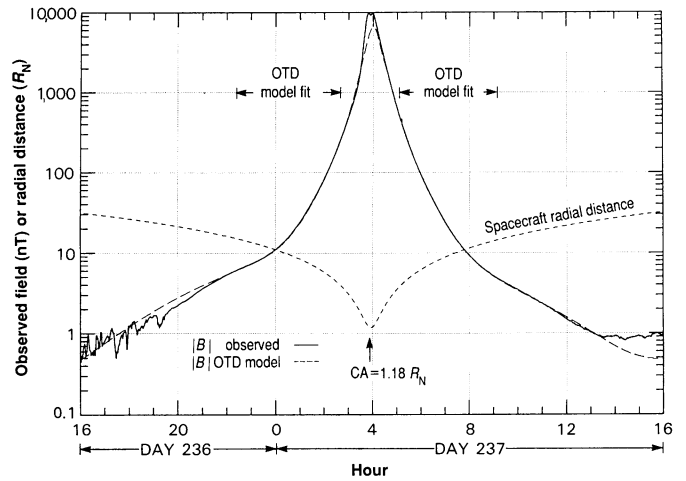
- 1) The boundary between the magnetosheath and the entry layer is marked by a discontinuity in the magnetic field direction, which can be identified with a crossing of the global magnetopause surface.
- 2) This directional discontinuity is associated with a local depression in the magnetic field intensity.
- 3) The magnitude of the magnetic field in the boundary layer is strongly fluctuating, whereas its direction is more stable.
- 4) The direction of the magnetic field in the boundary layer changes slowly, approaching the dipole configuration closer to the planet.

A similar magnetic field profile in the vicinity of Earth’s distant polar cusp was reported by Fairfield and Ness (9), who also observed high-frequently fluctuations in the magnetic field and a deficit in the field strength relative to the dipole. Enhanced magnetic field fluctuations and a deficit in the field strength relative to that of the OTD were also observed in the boundary layer at Neptune (see Figs. 1 and 3, respectively). If the boundary layer at Neptune is an entry layer, then the density and temperature in the layer should be comparable to that in the magnetosheath, the bulk speed should be low and irregular, and the density should drop abruptly at the inner edge of the layer. Plasma data are required to determine whether the boundary layer observed is a region of inflow, outflow, or stagnation.

Planetary magnetic field. Upon V2’s entry into the magnetosphere of Neptune (236/1800 to 236/1930), the observed magnitude of the magnetic field was between 1 and 2 nT (Fig. 3). The field then increased steadily by four orders of magnitude, reaching a maximum of 9950 nT just before CA at $1.18 R_N$ at 237/0355:39. The field, with a notable double peak, then steadily decreased with increasing radial distance from the planet, dropping to 1 nT at 237/1300 ($24 R_N$ distance). The brevity of this encounter, and the characteristics of the trajectory of V2, yielded an unusual spatial distribution of observations. Most of the variation in latitude and longitude occurred while V2 was relatively close to the planet, less than $4 R_N$. Between 4 and $20 R_N$, the latitude was bounded by 0° and -24° and the longitude remained between 275° and 75° W.

This longitude system is based on a planetary rotation period (10) of 16 hours 03 min, according to the Jet Propulsion Laboratory (JPL) trajectory data tape (SEDR)

Fig. 3. Comparison of the magnitude of the observed magnetic field (bold solid line) and OTD model field (long dashes) for a period of 24 hours centered on Neptune CA; radial distance of V2 from the planetary center (short dashes). The OTD model is based on vector averages of the field at 48-s intervals in the radial range of 4 to $15 R_N$.



issued after encounter. In this system, the spacecraft was at 160° W at CA. The Neptune pole position is defined by a right ascension of 298.85° , declination of 42.42° , as given in the 14 August 1989 JPL distribution of the physical constants.

An OTD representation has been adopted for the preliminary model of Neptune’s magnetic field. This representation is well suited for studies of magnetospheric structure in those regions where the field is mainly dipolar, $R > 4 R_N$. Closer to Neptune, the OTD is not a good approximation to the field; significant higher order multipoles or local sources, or both (as yet undetermined), cannot be neglected. For this initial report, we determined the best fitting OTD by systematically varying its location to obtain a minimum rms residual, while simultaneously allowing the magnitude and orientation of the dipole to vary. Averages of the vector field at 48-s intervals at radial distances of 4 to $15 R_N$ were used to determine the model.

The OTD model so obtained has a dipole moment of $0.133 \text{ G} \cdot R_N^3$, a dipole tilt (with respect to the rotation axis) of 46.8° toward 79.5° W. (The dipole harmonic terms are: $g_1^0 = 9100 \text{ nT}$, $g_1^1 = 1760 \text{ nT}$, $h_1^1 = -9520 \text{ nT}$. The orientation of the dipole is such that the positive pole is in Neptune’s northern hemisphere as defined by the planet’s angular momentum vector. Thus, field lines are directed outward of the northern hemisphere, as at Jupiter and Saturn, and opposite to the sense of the present-day geomagnetic field. The OTD center is displaced (offset) from the planet’s center by the surprisingly large value of $0.55 R_N$ (0.17, 0.46, and $-0.24 R_N$ in a right-handed coordinate system in which the positive z axis is aligned with the rotation axis and the x axis passes through the zero meridian).

This OTD model fits the magnetic field observations with an rms residual of 1.48 nT. Figure 3 compares the magnitude of the

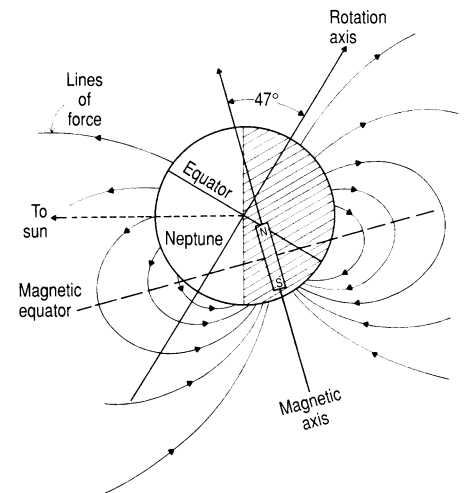


Fig. 4. Diagram of the OTD field lines of Neptune in the meridian plane containing the OTD center and the rotation axis, illustrating the effects of the large dipole tilt and offset on the location of the magnetic equator and pole regions. This figure is an approximation (the OTD axis is actually inclined by 22° with respect to this plane).

observed field with that obtained from the OTD model for 1 day centered about CA, corresponding to radial distances less than $30 R_N$. The OTD model fits the data remarkably well, even considerably outside the radial range of observations (4 to $15 R_N$) used in the determination of the model. A progressively increasing difference between the OTD model and the observed field is very evident near CA, in a region where the field is nondipolar and the OTD model is not applicable.

A schematic diagram of the approximate configuration of the dipole magnetic field is shown in Fig. 4. This planetary field appears similar, in many respects, to that of Uranus (4, 11). The magnetic field intensity on the planet’s surface may be expected to range from a low of $<0.1 \text{ G}$ to a maximum of $>1.0 \text{ G}$, because of the large spatial offset of the OTD. However, close to the planet, the

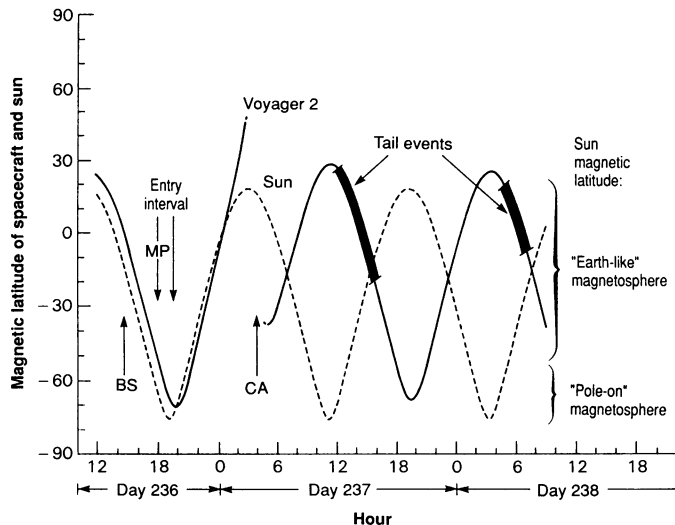
neglected but very substantial higher order multipole moments and possible localized sources will contribute significantly to the specifics of the field. Similarly, the intersection of the OTD poles with the planet's surface (north pole at 48°N, 57°W; south pole at 35°S, 278°W) may only be regarded as a guide in locating the true magnetic poles, particularly in the weak-field (northern) hemisphere, over which V2 passed closely. Indeed, like Uranus, this planet may have multiple magnetic dip equators (defined by $B_r = 0$) (B_r is the radial component of the magnetic field).

Magnetotail. After CA, V2 remained within the magnetosphere for 28 hours, exiting at a distance of 72 R_N (see Table 1). During this interval, the magnitude of the magnetic field decreased steadily and is well approximated by the OTD model from within 4 R_N to approximately 24 R_N (237/1300) (see Fig. 3). The direction of the field changed slowly from dipolar to tail-like beyond 15 R_N . During the intervals 237/1300–1600 and 238/0430–0814, the magnetic field was disturbed in a manner that suggests proximity to a tail plasma sheet. Between these disturbed intervals, the field decreased steadily but slowly from 1 to 0.5 nT.

The direction of the magnetic field remained tail-like during the remainder of the trajectory (Fig. 2). This apparent monopolar magnetic tail, however, is a result of a unique combination of the trajectory and the instantaneous tail configuration due to the large angular tilt of the OTD and the obliquity of Neptune. One can see that this is a plausible explanation by careful inspection of the time variation of the OTD magnetic latitude of V2 and the sun shown in Fig. 5.

The disturbed regions of the tail are associated with intervals in which the spacecraft is within 20° of the OTD equator. However, those regions do not occur symmetrically, being seen only after V2 has reached its maximum latitudinal excursion. The observation of the regions after V2 has reached its maximum latitude is interpreted to be due to the changing configuration from a pole-on magnetosphere to an Earth-like magnetosphere geometry. These two geometries are illustrated in Fig. 6 and summarized in studies by Voigt (12). The lower portions of this figure present the field line pole-on and Earth-like configurations in the noon-midnight meridian plane, which correspond to V2 entry into the magnetosphere (left) and exit from the magnetosphere (right). At the time V2 entered the magnetosphere, the phasing of the encounter with the rotation of the planet was such as to yield an almost pole-on magnetosphere configuration. This suggests the possibility of a cylindrically

Fig. 5. Plot of the variation of the magnetic latitude of V2 and the sun during the time interval from inbound bow shock (BS) to outbound magnetopause (MP) crossings. The inbound BS and MP crossings are indicated, along with the boundary layer entry interval. The time intervals for the two characteristic modes of solar wind interaction, Earth-like and pole-on, are also indicated.



shaped plasma "sheet" in the magnetic tail. This geometry changes progressively, as the planet rotates, until the configuration becomes Earth-like, as shown in the rightmost panels.

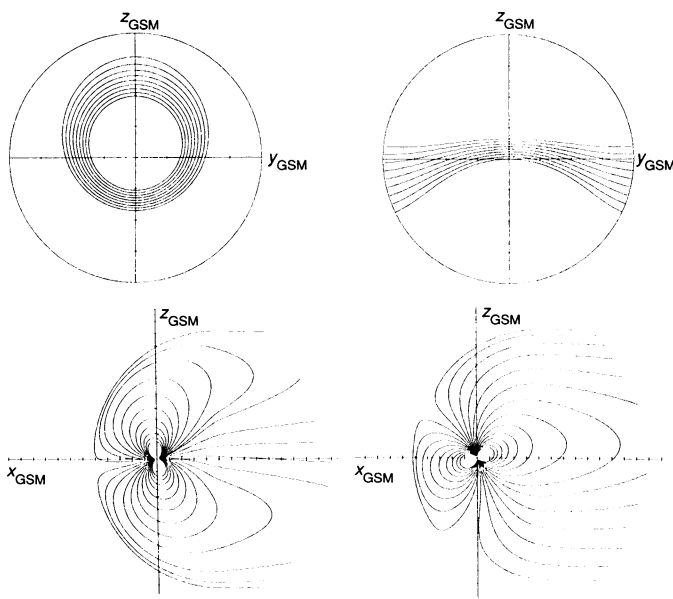
The continuously changing magnetospheric geometry, from pole-on to Earth-like, presents a very dramatic, dynamic magnetospheric structure. It is not possible at this early stage of the analysis to quantitatively describe this variation of magnetospheric structure, even for a steady solar wind flow. Changes in solar wind properties will also have even more dramatic effects on the configuration and dynamics of the Neptunian magnetosphere.

Satellite and ring interactions. The Voyager encounters at Jupiter, Saturn, and Uranus have shown that their moons and rings are very effective absorbers of magnetically trapped charged particles in their radiation belts. This is also the case at Neptune, where

such absorption features have been detected (13, 14). All of the new moons and the rings are located inside 4.75 R_N and will therefore be characterized by complex absorption features due to the complicated near magnetic field of Neptune. The OTD-derived L value for V2 and Triton outside 4 R_N is plotted as a function of time in Fig. 7. The L value for Triton sometimes exceeds 30 R_N , implying that Triton may be located well outside the inner magnetosphere of Neptune ($R < 15 R_N$) and indeed on field lines connected to the polar cusp or deep tail regions.

The interaction between the atmosphere and ionosphere of Triton (15, 16) and Neptune's magnetosphere leads to the creation of a modest plasma torus (17) with large dimensions, due to the large tilt of the global magnetic field of Neptune. Preliminary inspection of the magnetic field data, limited by as yet unresolved spacecraft attitude uncertainties around Triton CA (from

Fig. 6. Configurations of the magnetic field lines in the noon-midnight meridian plane (lower panels) and tail current stream lines (upper panels) forming the plasma "sheet" in the tail region; GSM, solar magnetospheric. The left panels refer to the pole-on geometry observed by V2 on entry into the Neptunian magnetosphere; the right panels refer to the Earth-like geometry observed by V2 on exit from the magnetosphere. The model magnetic field was developed by Voigt (12).



237/0700 to 237/1100) shows a stable magnetospheric field of Neptune but no signature attributable to Triton. In fact, in the assumed absence of an internal magnetic field of Triton, the atmosphere-ionosphere system requires an Alfvén wing interaction (18) at sub-Alfvénic Mach numbers, M_A . The sub-Alfvénic character of the flow is suggested by the absence of strong centrifugal instability of the magnetosphere near Triton's orbit.

The detectability of any Alfvén wings of Triton depends strongly on the location and distance of V2 from the wing. For a fully developed Alfvén wing, such as at Io (19), the relative disturbance field is given by Neubauer (20) as:

$$\frac{|\Delta B|}{B_0} = M_A \left(\frac{R_w}{r} \right)^2 \quad (1)$$

where B_0 is the undisturbed field, R_w is the radius of the wing, and r is the distance from the cylindrical wing. Hence, the detectability depends strongly on the orientation of the global magnetic field. Unfortunately, in this regard the geometry at V2 flyby was unfavorable because of the large tilt of the OTD.

Implications: Dynamo and internal structure. This admittedly limited model of the magnetic field of Neptune, with its highly tilted dipole (47°) and large equivalent offset ($0.55 R_N$), appears much like that of the planet Uranus. The presence of relatively large nondipolar contributions to the field is more clearly evidenced observationally at Neptune (Fig. 3) than at Uranus, owing to V2's closer approach to Neptune ($1.18 R_N$ as compared with $4.2 R_U$). Uranus and Neptune appear to occupy a separate and distinct subclass of planetary dynamos characterized by large dipole tilts and complex field geometries (quadrupole moment comparable to dipole). In contrast, Earth, Jupiter, and Saturn have fields with small dipole tilts ($<12^\circ$) and relatively small quadrupole contributions (less than 10% of the dipole). Mercury appears to also have a small tilt, but the quadrupole is undetermined (21).

The large offsets of the OTDs, or equivalently the large quadrupole moments, at Uranus and Neptune suggest dynamo generation in a region far removed from the planet's center (4), in a fluid and convecting "ice mantle" consisting of H_2O , ammonia (NH_3), and methane (CH_4). The "ice mantle" accounts for perhaps two-thirds of the total mass of the planets, according to contemporary models of the interior (22); the remainder resides in a small, central "rock" core of the high-temperature condensates and a modest H-He atmosphere. The electrical resistivity of the ice mantle, at-

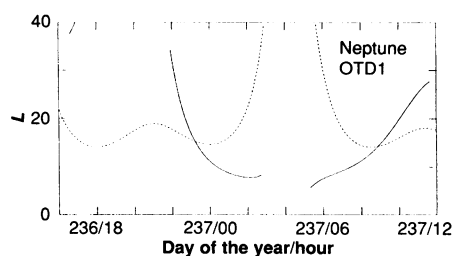


Fig. 7. Plot of the variation of the L value for Triton (dashed line) and V2 (solid line) based on the preliminary OTD model for Neptune's magnetic field. For the period during which V2 was within $4 R_N$ of the planet, the L values are not plotted because they are most likely not valid.

tributed to pressure-induced ionization of H_2O , is 2 to 20 ohm cm^{-1} (23). This is orders of magnitude less than that assumed for the dynamo regions of the other planets (24).

The similarity of the magnetic fields of Uranus and Neptune suggests that the large dipole tilt and offset are characteristics of dynamo generation in these bodies, a consequence of their unique interior composition and state, as suggested by Connerney *et al.* (11, 25). It now appears unlikely that the large tilt and offset of the Uranian field is related to that planet's uniquely large orbital obliquity (26). Less likely, now, is the proposal that V2 observed a dynamo at Uranus in the process of a field reversal (27), a process thought to produce such a field configuration in the terrestrial example.

The most significant difference between the magnetic fields of Neptune and Uranus evident at present appears to be the difference in the magnitudes of the dipole moments: Neptune's is $2 \times 10^{27} \text{ G-cm}^3$, and Uranus's is $3.8 \times 10^{27} \text{ G-cm}^3$. For planets of similar size with a similar interior composition and state, one might expect the magnitude of the dipole moment to reflect the amount of energy available to power the dynamo. Because the internal energy source is much greater at Neptune than at Uranus (28), the ratio of the dipole moments appears contrary to expectation. However, in the case of Neptune and Uranus, with their relatively large higher order moments, it appears that the bulk of the energy of the dynamo may reside in the higher order moments of the field, for which we have insufficient data to make a meaningful comparison. And there may be appreciable deviations from quantitative similarity between Uranus and Neptune, with respect to the higher order multipoles of the global fields.

Conclusions. V2's encounter very serendipitously occurred simultaneous with the rotation phase of Neptune so that, in association with its oddly tilted magnetic field, the

unique and previously unexplored configuration of a pole-on magnetosphere in the solar wind was observed. It is expected that future study of the eccentric magnetic field of Neptune will shed much light on the dynamics of its radiation belt structure, the dynamo generation of magnetic fields, and the interior structures of both Neptune and Uranus. Neptune presents a most intriguing magnetospheric configuration, whose observed variations will provide profound tests of theoretical models of solar wind interaction with planetary magnetic fields.

REFERENCES AND NOTES

1. K. W. Behannon *et al.*, *Space Sci. Rev.* **21**, 235 (1977).
2. N. F. Ness *et al.*, *Science* **206**, 966 (1979).
3. N. F. Ness *et al.*, *ibid.* **215**, 558 (1982); M. H. Acuña, J. E. P. Connerney, N. F. Ness, *J. Geophys. Res.* **88**, 8771 (1983).
4. N. F. Ness *et al.*, *Science* **233**, 85 (1986); J. E. P. Connerney, M. H. Acuña, N. F. Ness, *J. Geophys. Res.* **92**, 15329 (1987).
5. N. F. Ness, M. H. Acuña, K. W. Behannon, F. M. Neubauer, *J. Geophys. Res.* **87**, 1369 (1982).
6. T. W. Hill, in *Uranus and Neptune*, J. T. Berstrahl, Ed. (Publication CP-2330, NASA, Washington, DC, 1984), p. 497, and references therein; I. de Pater and C. K. Goertz, *Geophys. Res. Lett.* **16**, 97 (1989).
7. S. A. Curtis and N. F. Ness, *J. Geophys. Res.* **91**, 11003 (1986); A. J. Dessler and R. B. Sandel, *Geophys. Res. Lett.* **16**, 957 (1989); J. A. Van Allen, in *Essays in Space Science*, R. Ramaty, T. L. Cline, J. F. Ormes, Eds. (Publication CP-2464, NASA, Washington, DC, 1987), pp. 1-18.
8. G. Paschmann, G. Haerendel, N. Schopke, H. Rosenbauer, P. C. Hedgecock, *J. Geophys. Res.* **81**, 2883 (1976); R. Lundin, *Space Sci. Rev.* **48**, 263 (1988), and references therein.
9. D. H. Fairfield and N. F. Ness, *J. Geophys. Res.* **77**, 611 (1972).
10. J. W. Warwick *et al.*, *Science* **246**, 1498 (1989).
11. J. E. P. Connerney, M. H. Acuña, N. F. Ness, *J. Geophys. Res.* **92**, 15,329 (1987).
12. G.-H. Voigt, *Planet. Space Sci.* **29**, 1 (1981); ———, T. W. Hill, A. J. Dessler, *Astrophys. J.* **266**, 390 (1983); G.-H. Voigt, *J. Geophys. Res.* **89**, 2169 (1984); ———, K. W. Behannon, N. F. Ness, *ibid.* **92**, 15337 (1987).
13. S. M. Krimigis *et al.*, *Science* **246**, 1483 (1989).
14. E. C. Stone *et al.*, *ibid.*, p. 1489.
15. L. Broadfoot *et al.*, *ibid.*, p. 1459.
16. G. L. Tyler *et al.*, *ibid.*, p. 1466.
17. J. W. Belcher *et al.*, *ibid.*, p. 1478.
18. F. M. Neubauer, *Adv. Space Res.*, in press.
19. M. H. Acuña, F. M. Neubauer, N. F. Ness, *J. Geophys. Res.* **86**, 8513 (1981); J. W. Belcher, *Science* **238**, 170 (1987).
20. F. M. Neubauer, *J. Geophys. Res.* **85**, 1171 (1980).
21. J. E. P. Connerney and N. F. Ness, in *Mercury*, F. Vilas, C. Chapman, M. S. Matthews, Eds. (Univ. of Arizona Press, Tucson, 1988), pp. 494-513.
22. W. B. Hubbard and J. J. MacFarlane, *J. Geophys. Res.* **85**, 225 (1980); M. Torbet and R. Smoluchowski, *Geophys. Res. Lett.* **6**, 675 (1979); M. Podolak and R. T. Reynolds, *Icarus* **46**, 40 (1981).
23. W. J. Nellis *et al.*, *Science* **240**, 779 (1988); R. Smoluchowski, *Astrophys. J.* **200**, L119 (1975).
24. D. J. Stevenson, *Rep. Prog. Phys.* **46**, 555 (1983).
25. R. Hide, *Geophys. Astrophys. Fluid Dyn.* **44**, 207 (1988).
26. D. J. Stevenson, *Sky Telescope* (May 1986), p. 481.
27. M. Schulz and G. A. Paulikas, *Adv. Space Res.*, in press.
28. R. F. Lowenstein, D. A. Harper, H. Moseley, *Astrophys. J.* **218**, L145 (1977).
29. We thank our colleagues at Goddard Space Flight Center (GSFC) and those on Voyager cosmic rays, low-energy charged particles, plasma, planetary ra-

dio astronomy, and plasma waves investigations for discussions of these early results. We also thank J. A. Van Allen for comments on these results. We thank the entire Voyager Project staff at JPL for the success of the mission and their support of our investigation, especially G. Sisk, E. Franzgrote, N. Toy, H. Woo, O. Divers, and W. McDougal. For

support at GSFC we thank W. Mish and his data-processing and analysis team, particularly T. Vollmer, R. Kennan, P. Hodge, P. Harrison, J. Jones, T. Carleton, J. Annen, G. Burgess, J. Byrnes, S. Kempler, L. Moriarty, F. Ottens, A. Silver, and R. Thompson; C. Moyer, J. Scheifele, J. Seek, and E. Worley for contributions to the design, develop-

ment, and testing of the hardware; and F. Hunsaker and S. Myers for graphics support. F.M.N. was supported financially by the German Ministry of Science and Technology. N.F.N. was supported in part by JPL contract 957921.

25 October 1989; accepted 15 November 1989

Plasma Observations Near Neptune: Initial Results from Voyager 2

J. W. BELCHER, H. S. BRIDGE, F. BAGENAL, B. COPPI, O. DIVERS, A. EVIATAR, G. S. GORDON, JR., A. J. LAZARUS, R. L. MCNUTT, JR., K. W. OGILVIE, J. D. RICHARDSON, G. L. SISCOE, E. C. SITTLER, JR., J. T. STEINBERG, J. D. SULLIVAN, A. SZABO, L. VILLANUEVA, V. M. VASYLIUNAS, M. ZHANG

The plasma science experiment on Voyager 2 made observations of the plasma environment in Neptune's magnetosphere and in the surrounding solar wind. Because of the large tilt of the magnetic dipole and fortuitous timing, Voyager entered Neptune's magnetosphere through the cusp region, the first cusp observations at an outer planet. Thus the transition from the magnetosheath to the magnetosphere observed by Voyager 2 was not sharp but rather appeared as a gradual decrease in plasma density and temperature. The maximum plasma density observed in the magnetosphere is inferred to be 1.4 per cubic centimeter (the exact value depends on the composition), the smallest observed by Voyager in any magnetosphere. The plasma has at least two components; light ions (mass, 1 to 5) and heavy ions (mass, 10 to 40), but more precise species identification is not yet available. Most of the plasma is concentrated in a plasma sheet or plasma torus and near closest approach to the planet. A likely source of the heavy ions is Triton's atmosphere or ionosphere, whereas the light ions probably escape from Neptune. The large tilt of Neptune's magnetic dipole produces a dynamic magnetosphere that changes configuration every 16 hours as the planet rotates.

NEPTUNE'S MAGNETOSPHERE IS the last to be visited by a Voyager spacecraft. As at Uranus, the very existence of a magnetosphere at Neptune was in question until the Voyager 2 flyby. This encounter was unique since Voyager approached much closer to Neptune, 1.2 Neptunian radii ($1 R_N = 24,765$ km), than it had to any other planet and also made the first pass over the rotational pole of a giant planet. In this report we describe observations of the spatial distribution and physical properties of the plasma near Neptune.

The Voyager plasma science (PLS) experiment measured positive ions and electrons with energies per charge from 10 to 5950 V (1). These observations were obtained simultaneously in four modulated-grid Faraday cup detectors. Three of these detectors (A, B, and C sensors) pointed approximately toward Earth and were ideally oriented for measuring solar wind and magnetosheath plasma. The D sensor "looked" at right angles to this direction and was oriented via spacecraft rolls to look into the corotation direction (toward plasma moving azimuthally in the direction of Neptune's rotation) inbound and outbound from the planet and upward (away from the planet) near closest approach. Four different measurement modes were used. A high-resolution M mode ($\Delta E/E = 3.6\%$) and a low-resolution L mode ($\Delta E/E = 29\%$) measure ion currents over the entire energy-per-charge range of the instrument (10 to 5950 V). A high-energy E2 mode (140 to 5950 eV) and low-energy E1 mode (10 to 140 eV) measure electron currents with energy resolutions $\Delta E/E$ of 29 and 9.9%,

respectively. The nominal time resolution of the data shown here is 48 s for ion data and 96 s for electron data.

Figure 1 shows an overview of the plasma measurements near Neptune, including the ion currents measured in the C sensor, electron currents, and electron densities measured along the spacecraft trajectory, which is shown in Fig. 2. The currents plotted are summations over energy per charge from 10 to 140 V for electrons and 10 to 1000 V for ions. The analysis used to compute the electron density profile is similar to that used at Uranus (2) except that, because of the low fluxes at higher energies, only E1 spectra were used.

Bow shock and magnetopause. The bow shock and magnetopause crossings are labeled in Fig. 1. A list of crossing times is given in Table 1, and the locations of these crossings on the spacecraft trajectory are indicated in Fig. 2. Multiple crossings may have occurred outbound, leading to some uncertainty in the quoted times. In general, these crossing times agree fairly well with identifications made by means of the magnetometry (MAG) data (3). Upstream of the bow shock the solar wind protons were moving as a cold beam with a streaming energy of 850 eV. On crossing the shock, the ions slowed down and were heated to several hundred electron volts. The total flux of ions remained roughly constant across the shock and into the magnetosheath. Electrons, which were too cold to be observed by the PLS instrument in the solar wind, were heated at the shock and were detected in the low-energy electron channels in the magnetosheath. The model curves in Fig. 2 represent the bow shock and magnetopause surfaces; they are conic sections (hyperbola and ellipse, respectively) fitted to the inbound and outbound bow shock and magnetopause crossings and constrained in shape to agree with gas dynamic analogs (4). The large tilt and offset of Neptune's magnetic field (3) produce a time-variable magnetic field configuration, resulting in periodic variations in the magnetospheric shape as the planet rotates. Comparison of the bow shock shape with those of the other planets shows that Neptune's bow shock is similar to Jupiter's and less flared than Earth's and Saturn's. The solar wind ion density, tem-

J. W. Belcher, H. S. Bridge, B. Coppi, G. S. Gordon, Jr., A. J. Lazarus, R. L. McNutt, Jr., J. D. Richardson, J. T. Steinberg, J. D. Sullivan, A. Szabo, L. Villanueva, M. Zhang, Massachusetts Institute of Technology, Cambridge, MA 02139.

F. Bagenal, University of Colorado, Boulder, CO 80309.

O. Divers, Jet Propulsion Laboratory, California Institute of Technology, Pasadena, CA 91109.

K. W. Ogilvie and E. C. Sittler, Jr., National Aeronautics and Space Administration Goddard Space Flight Center, Greenbelt, MD 20770.

G. L. Siscoe, University of California, Los Angeles, CA 90024.

A. Eviatar, Tel Aviv University, Tel Aviv, Israel.

V. M. Vasylunas, Max-Planck-Institut für Aeronomie, Katlenburg-Lindau, Federal Republic of Germany.